

## Collisional properties of cold spin-polarized metastable neon atoms

P. Spoden,<sup>1</sup> M. Zinner,<sup>1</sup> N. Herschbach,<sup>1</sup> W. J. van Drunen,<sup>1</sup> W. Ertmer,<sup>1</sup> and G. Birkel<sup>1,2</sup>

<sup>1</sup>*Institut für Quantenoptik, Universität Hannover, Welfengarten 1, D-30167 Hannover*

<sup>2</sup>*Institut für Angewandte Physik, Technische Universität Darmstadt, Schlossgartenstr. 7, D-64289 Darmstadt*

(Dated: November 5, 2018)

We measure the rates of elastic and inelastic two-body collisions of cold spin-polarized neon atoms in the metastable  $^3P_2$  state for  $^{20}\text{Ne}$  and  $^{22}\text{Ne}$  in a magnetic trap. From particle loss, we determine the loss parameter of inelastic collisions  $\beta = 6.5(18) \times 10^{-12} \text{ cm}^3 \text{ s}^{-1}$  for  $^{20}\text{Ne}$  and  $\beta = 1.2(3) \times 10^{-11} \text{ cm}^3 \text{ s}^{-1}$  for  $^{22}\text{Ne}$ . These losses are caused by ionizing (i.e. Penning) collisions and occur less frequently than for unpolarized atoms. This proves the suppression of Penning ionization due to spin-polarization. From cross-dimensional relaxation measurements, we obtain elastic scattering lengths of  $a = -180(40) a_0$  for  $^{20}\text{Ne}$  and  $a = +150_{-50}^{+80} a_0$  for  $^{22}\text{Ne}$ , where  $a_0 = 0.0529 \text{ nm}$ .

PACS numbers: 34.50.-s, 34.50.Fa, 32.80.Pj, 82.20.Pm

The experimental investigation of the collisional interaction of cold and ultracold atoms has been a driving force for important new physics in recent years. The successful demonstration of Bose-Einstein condensation (BEC) in dilute atomic gases certainly is one of the most prominent examples of this development [1]. Other examples are the realization of Fermi-degenerate systems (see [2] for an overview) or the generation of molecular BECs [3]. The collisional properties of ultracold atoms critically determine the achievability of quantum-degenerate systems, their stability, their coherence properties, and the characteristics of collective phenomena (see [2, 4] for a review) and thus deserve detailed investigation. All along, experimental work on cold collisions for an additional atomic species has initiated a new line of exciting research. Special interest nowadays arises from the investigation of non-alkali systems, such as  $\text{He}^*$  [5, 6],  $\text{Yb}$  [7],  $\text{Cr}$  [8, 9], with their specific interaction properties.

An important novel class of atomic species in this respect are cold and ultracold rare gas atoms in metastable triplet states ( $\text{RG}^*$  atoms). Due to their high internal energy, these atoms show collisional properties and experimental provisions absent in other atomic systems. Important results have already been achieved in  $\text{He}^*$ , such as the realization of BEC [5, 6], the implementation of highly efficient electronic detection of quantum-degenerate atomic samples [5], its application to the determination of the elastic scattering length [10], and the formation of  $\text{He}_2^*$  dimers in purely long-range states [11]. With this paper, we extend the experimental investigation of cold collisions of metastable atoms to the case of neon.

Compared to helium, neon has a more complex internal structure. This causes for example the occurrence of more than one metastable triplet state and of anisotropic electrostatic interaction potentials, which influence the dynamics of elastic and inelastic collisions [12, 13]. Inelastic interactions of  $\text{RG}^*$  atoms are particularly interesting due to their specific exoergic character. With high probability,  $\text{RG}^*$  atoms exhibit Penning ionization reac-

tions [14], where one of the atoms is deexcited to the ground state, the other atom is ionized, and an electron is released. Penning ionization may be suppressed if the colliding atoms are spin-polarized to a spin-stretched state since then Penning ionization does not conserve the spin quantum number. The extent of suppression depends critically on anisotropic contributions to the interaction. In the case of  $\text{He}^*$  these contributions are small and ionization is suppressed by four to five orders of magnitude [10]. The heavier rare gases however have stronger anisotropic contributions, since the excitation of an electron to the metastable state creates a  $p^5$ -core with non-zero orbital angular momentum. Indeed, no suppression of Penning ionization was observed in  $\text{Xe}^*$  [15]. For neon, Doery et al. calculate suppression ratios between 1 and  $10^4$ , which depend most sensitively on exact interaction potentials [12], which were not available at the time. Experimental investigations are needed, but so far measurements of the ionization rate have only been reported for unpolarized atoms [16, 17, 18].

In this paper, we present the experimental determination of the rates of elastic and inelastic collision of spin-polarized bosonic  $^{20}\text{Ne}$  and  $^{22}\text{Ne}$  atoms in the  $J=m_J=+2$  substate of the metastable  $^3P_2$  state. For both isotopes, we determine the elastic scattering length  $a$ , the loss parameter of inelastic collisions  $\beta$ , and demonstrate the suppression of Penning ionization due to spin-polarization.

In our experiment, we capture  $\text{Ne}^*$  atoms in a magneto-optical trap from a Zeeman-decelerated atomic beam [19]. After optical pumping into the  $m_J=+2$  state, the atoms are transferred into a magnetic Ioffe-Pritchard trap with radial gradient of  $295 \text{ G/cm}$  and axial curvature of  $215 \text{ G/cm}^2$ . As a last step of preparation, we apply one-dimensional Doppler cooling [20], where the trapped atoms are irradiated by two  $\sigma^+$  polarized laser beams along the symmetry axis of the magnetic trap. For this purpose, we operate the trap with an offset magnetic field of  $25 \text{ G}$ . The vibrational frequencies, measured with  $^{20}\text{Ne}$ , are  $\omega_x = 2\pi \times 80(1) \text{ s}^{-1}$  in axial direction and  $\omega_r = 2\pi \times 186(1) \text{ s}^{-1}$  in radial direction. By this prepara-

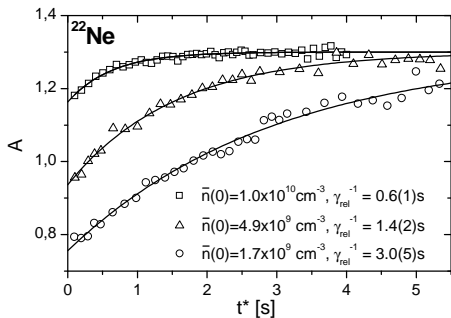


FIG. 1: Cross-dimensional relaxation of the aspect ratio of  $^{22}\text{Ne}$  ensembles for different initial densities  $\bar{n}(0)$ . Higher densities lead to shorter relaxation times  $\gamma_{\text{rel}}^{-1}$ . The lines are fits according to Eq. 1. During relaxation  $\bar{n}$  and  $\bar{T}$  change. We compensate for the resulting change in  $\gamma_{\text{rel}}$  by using the rescaled time  $t^*(t) = \int_0^t (\bar{n}(t') \bar{v}(t')) / (\bar{n}(0) \bar{v}(0)) dt'$ , similar to [22].

ration we obtain typical temperatures of  $T_x = 450 \mu\text{K}$  in axial and  $T_r = 600 \mu\text{K}$  in radial direction. A typical atom cloud contains  $N = 2 \times 10^8$  atoms, at a mean density  $\bar{n} = 4 \times 10^{10} \text{cm}^{-3}$ , the latter being the ensemble average of the number density  $n(\vec{r})$ :  $\bar{n} = N^{-1} \int n^2(\vec{r}) d^3r$ . By a Stern-Gerlach experiment, we could verify that the spin-polarization persists during Doppler cooling. We could not detect any atoms in the  $J=2$ ,  $m_J \leq 1$  substates, from which we deduce a lower bound of 95% for the atom population in the  $m_J=2$  substate.

As one-dimensional Doppler cooling in the magnetic trap gives different temperatures,  $T_x < T_r$ , we obtain an ensemble out of equilibrium. In each dimension however, potential and kinetic energy are balanced such that  $\omega_{x(r)} \sigma_{x(r)} = \sqrt{k_B T_{x(r)} / m}$ , where  $\sigma_{x(r)}$  is the spatial width in axial (radial) direction and  $\sqrt{k_B T_{x(r)} / m}$  the velocity spread, with Boltzmann's constant  $k_B$ , and the atomic mass  $m$ . After cooling, the trapped ensemble trends back to equilibrium, which can be observed by a changing aspect ratio of the spatial distribution. In parallel, the number of atoms decreases with time and their mean temperature increases. We observe heating rates which are density dependent and range from a few  $\mu\text{K/s}$  up to  $50 \mu\text{K/s}$  for increasing densities.

In general, collision rates depend on the atom cloud's density and temperature. We derive  $\bar{n}$ ,  $T_x$ , and  $T_r$  from absorption images which are taken between 0.5 and 2 ms after switching off the magnetic trap. For the determination of these parameters, statistical uncertainties (typically 2 – 3%) are negligible as compared to systematic uncertainties. Uncertainties are given as one standard deviation and represent the quadrature sums of statistical and systematic contributions, dominated by the systematic uncertainty in density ( $23\% \leq \Delta\bar{n}/\bar{n} \leq 28\%$ ).

We determine the rates of elastic collisions from cross-dimensional relaxation measurements [8, 21, 22]. The equilibrating transfer of energy from the radial to the

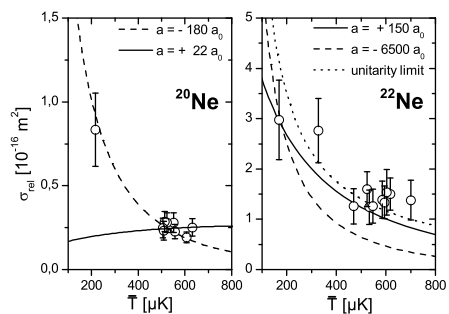


FIG. 2: Effective relaxation cross sections  $\sigma_{\text{rel}}$  obtained from cross-dimensional relaxation measurements and calculations: (left) For  $^{20}\text{Ne}$  we obtain a scattering length of  $a = -180(40) a_0$ . The measurements between 500 and 700  $\mu\text{K}$  are also consistent with a positive  $a = +22(5) a_0$ ; (right) The large  $\sigma_{\text{rel}}$ -values of  $^{22}\text{Ne}$  are close to the unitarity limit. Our data agree best with theory for  $a = +150_{-50}^{+80} a_0$ . We can rule out negative scattering lengths since theory cannot match our data, as exemplified for  $a = -6500 a_0$  (see text).

axial dimension changes the atom cloud's aspect ratio  $A(t)$ , according to

$$\dot{A}(t) = -\gamma_{\text{rel}}(A(t) - A_{\text{eq}}). \quad (1)$$

Here,  $A_{\text{eq}}$  is the equilibrium aspect ratio and  $\gamma_{\text{rel}}$  the relaxation rate. We observe reequilibration of  $^{20}\text{Ne}$  and  $^{22}\text{Ne}$  (Fig. 1) for different initial densities  $\bar{n}(0)$  and find relaxation rates which are directly proportional to  $\bar{n}(0)$  [18]. Hence relaxation is predominantly caused by collisions and ergodic mixing is of no relevance for our determination of  $\gamma_{\text{rel}}$  [23]. Therefore, we can describe the relaxation rate of the atomic ensemble by an effective relaxation cross section  $\sigma_{\text{rel}}$ ,

$$\gamma_{\text{rel}} = \sigma_{\text{rel}} \bar{n} \bar{v}, \quad (2)$$

where  $\bar{v} = (16k_B \bar{T} / \pi m)^{1/2}$  is the average relative velocity of the colliding atoms, with the mean temperature  $\bar{T} = \frac{1}{3}(T_x + 2T_r)$ .

Since the relaxation process is driven stronger by collisions with high relative velocity, Kavoulakis et al. have derived  $\sigma_{\text{rel}} \propto \langle \sigma_{\text{el}}(v) v \rangle_{\text{nst.}}$  from a non-standard thermal average of the elastic collision cross section  $\sigma_{\text{el}}(v)$ , (Eqs. (72) and (88) in [24]), where  $v$  denotes the relative velocity of the colliding atoms. Thereby  $\sigma_{\text{rel}}$  becomes a function of scattering length  $a$  and temperature:  $\sigma_{\text{rel}} = \sigma_{\text{rel}}(a, \bar{T})$ .

Figure 2 shows the relaxation cross sections of  $^{20}\text{Ne}$  and  $^{22}\text{Ne}$  as a function of temperature [25]. We have prepared atom clouds at different temperatures either by varying the efficiency of Doppler cooling, or by an additional adiabatic expansion within the trap. The temperature assigned to each measurement is the average of temperatures  $\bar{T}(t)$  weighted with  $\dot{A}(t)$ . This procedure reflects that the period of fastest change in  $A(t)$  is most important for the extraction of  $\gamma_{\text{rel}}$  [26].

In our measurements, relaxation is dominated by s-wave collisions between spin-polarized atoms, as the centrifugal barrier for d-waves is  $k_B \times 5.6$  mK in energy. In the temperature range we explore, the elastic scattering cross section depends on both the magnitude *and* the sign of the scattering length  $a$ , as opposed to the case of ultracold collisions, where  $\sigma_{\text{el}} \rightarrow 8\pi a^2$ . To analyze the data, we use the temperature dependence of  $\sigma_{\text{rel}}(a, \bar{T})$  which we derive from numerical calculations: we start by calculating  $\sigma_{\text{el}}(v)$  as a function of  $v$  for different input values of  $a$  by solving the radial Schrödinger equation. With the non-standard average  $\langle \sigma_{\text{el}}(v) v \rangle_{\text{nst.}}$  we calculate  $\sigma_{\text{rel}}(a, \bar{T})$  for temperatures between 100 and 800  $\mu\text{K}$  (lines in Fig. 2) and determine the scattering length by fitting these curves to the experimental data ( $\chi^2$  minimization procedure).

These calculations are based on the short-range ab-initio potentials given by Kotochigova et al. [27], and the long-range van-der-Waals potentials given by Derevianko et al. [28]. We treat the collision process by a single-channel calculation, instead of including the five potentials involved, for three reasons: (i) the sensitivity of the  $v$ -dependence of  $\sigma_{\text{el}}(v)$  on the short-range potentials is negligible (see also [8, 13]); (ii) the 4% uncertainty in the van-der-Waals coefficients for the different potentials involved is comparable to their differences [28]; (iii) the variation in the calculated  $\sigma_{\text{rel}}(a, \bar{T})$  caused by these differences are negligible when compared to experimental uncertainties in the measurement of  $\sigma_{\text{rel}}$ .

For  $^{20}\text{Ne}$ , we obtain a negative scattering length of  $a = -180(40) a_0$ , with Bohr's radius  $a_0 = 0.0529$  nm. Between 500 and 650  $\mu\text{K}$ , our data are also consistent with a positive value of  $a = +22(5) a_0$ . The sign of the scattering length is determined by the measurements at  $\bar{T} \approx 200 \mu\text{K}$ , giving a 74 times higher probability for  $a = -180 a_0$  than for  $a = +22 a_0$ . For  $^{22}\text{Ne}$ , we obtain relaxation cross sections  $\sigma_{\text{rel}}$  which are three to five times larger as compared to  $^{20}\text{Ne}$  (Fig. 2). We obtain  $a = +150_{-50}^{+80} a_0$ . Due to the proximity of the  $\sigma_{\text{rel}}$ -data to the unitarity limit, the extracted  $a$  is less precise than in the case of  $^{20}\text{Ne}$ . Our calculations show that the relaxation cross sections for  $a < 0$  do not match our data. We exemplify this by including a plot of  $\sigma_{\text{rel}}$  for  $a = -6500 a_0$  in Fig. 2. All curves calculated for  $-6500 a_0 < a < 0$  lie below this curve, and thus disagree with our data. We therefore conclude that the scattering length of  $^{22}\text{Ne}$  is positive.

From atom loss in the magnetic trap, we determine the rate of binary inelastic collisions of a spin-polarized ensemble. The decrease in atom number  $N(t)$  (Fig. 3, left) stems from one-body losses ( $\propto N$ ) and two-body losses ( $\propto N^2$ ). We have no signature of higher order loss processes in our measurements. One body-losses with rate  $\alpha$  are mainly caused by the 14.73 s lifetime of the  $^3\text{P}_2$  state [19] and by background gas collisions. Two-body losses depend on the probability of two atoms to collide

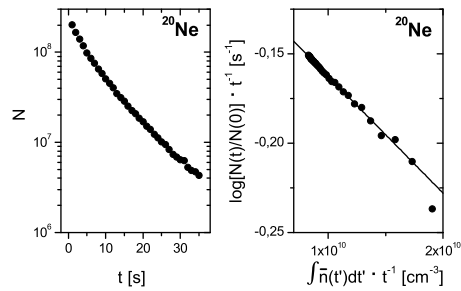


FIG. 3: (left) Atom loss of a spin-polarized  $^{20}\text{Ne}$  ensemble. Initially,  $2 \times 10^8$  atoms were trapped at a mean density  $\bar{n} = 2 \times 10^{10} \text{ cm}^{-3}$ . (right) Data presented according to Eq. (4) and a linear fit giving a one body loss rate  $\alpha = (10.3(3) \text{ s})^{-1}$  and a loss constant  $\beta = 6.5(18) \times 10^{-12} \text{ cm}^3 \text{ s}^{-1}$ .

( $\propto n^2(\vec{r})$ ) and on the loss parameter  $\beta$ . The decay of the particle number is described by

$$\frac{d}{dt} N(t) = -\alpha N(t) - \beta \frac{N^2(t)}{V_{\text{eff}}(t)}, \quad (3)$$

with the effective volume  $V_{\text{eff}} = N/\bar{n}$ . We find that  $V_{\text{eff}}$  increases due to heating, so that an explicit solution of Eq. (3) requires assumptions on the heating mechanisms involved. We circumvent this by formally integrating Eq. (3) and obtain a linear relation between quantities, which are easily derived from measured data:

$$\frac{1}{t} \log \frac{N(t)}{N(0)} = -\alpha - \beta \left( \frac{1}{t} \int_0^t \bar{n}(t') dt' \right). \quad (4)$$

The constant offset in this relation is the one-body loss rate  $\alpha$  and the slope is the two-body loss parameter  $\beta$ .

By presenting the data of a trap loss measurement (Fig. 3 (left)) according to Eq. (4), we find the expected linear dependence (Fig. 3 (right)). From this, we get the one-body decay rate  $\alpha^{-1} = 10.3(3) \text{ s}$ , and the two-body loss parameter  $\beta = 6.5(18) \times 10^{-12} \text{ cm}^3 \text{ s}^{-1}$ . The uncertainty in  $\beta$  is dominated by the systematic uncertainty in  $\bar{n}$ . Comparing  $\beta$  to the loss parameter of an unpolarized ensemble  $\beta_{\text{unpol}} = 2.5(8) \times 10^{-10} \text{ cm}^3 \text{ s}^{-1}$  [17, 18], we obtain the suppression of inelastic collisions due to spin-polarization  $\beta_{\text{unpol}}/\beta = 38(16)$  for  $^{20}\text{Ne}$ .

We get a second independent measurement of the rate of inelastic collisions from observed heating rates. Besides other possible heating mechanisms, two-body loss leads to intrinsic heating: these collisions happen most likely in the center of the trap. Therefore, the average energy carried away by a lost atom is less than the mean energy per trapped atom. By fitting the resulting heating rate  $\dot{\bar{T}}/\bar{T} = \beta\bar{n}/4$  [29] to the rising mean temperature  $\bar{T}$ , we obtain  $\beta_{\text{heat}} = 7(2) \times 10^{-12} \text{ cm}^3 \text{ s}^{-1}$ . This value agrees well with the result from the trap loss measurement and indicates that other heating mechanisms do not contribute significantly to observed heating rates.

TABLE I: Summary of collision parameters: effective relaxation cross section  $\sigma_{\text{rel}}$  for  $T = 200$  and  $550\mu\text{K}$ , scattering length  $a$ , two-body loss parameters  $\beta$  and  $\beta_{\text{unpol}}$  for polarized and unpolarized atoms and their suppression ratio.

		$^{20}\text{Ne}$	$^{22}\text{Ne}$
$\sigma_{\text{rel}}(\approx 200\mu\text{K})$	$[10^{-17} \text{ m}^2]$	8(2)	30(8)
$\sigma_{\text{rel}}(\approx 550\mu\text{K})$	$[10^{-17} \text{ m}^2]$	2.8(7)	13(3)
$a$	$[a_0]$	-180(40)	$+150_{-50}^{+80}$
$\beta$	$[10^{-12} \text{ cm}^3\text{s}^{-1}]$	6.5(18)	12(3)
$\beta_{\text{unpol}}$	$[10^{-12} \text{ cm}^3\text{s}^{-1}]$	250(80)	80(50)
$\beta_{\text{unpol}}/\beta$		38(16)	7(5)

We performed similar measurements with  $^{22}\text{Ne}$  at an initial atom number of  $9 \times 10^7$  ( $\bar{n} = 1.4 \times 10^{10} \text{ cm}^{-3}$ ) yielding a one-body decay rate of  $\alpha^{-1} = 14.5(2) \text{ s}$ . We find a loss parameter of  $\beta = 1.2(3) \times 10^{-11} \text{ cm}^3\text{s}^{-1}$  from the decay measurement, and  $\beta_{\text{heat}} = 1.3(3) \times 10^{-11} \text{ cm}^3\text{s}^{-1}$  from observed heating. With a loss parameter  $\beta_{\text{unpol}} = 8(5) \times 10^{-11} \text{ cm}^3\text{s}^{-1}$  [18] for unpolarized atoms, the suppression of two-body losses is  $\beta_{\text{unpol}}/\beta = 7(5)$  for  $^{22}\text{Ne}$ .

In an additional experiment, we simultaneously detected atoms with absorption imaging and measured the rate of ions escaping from a cloud of trapped  $^{22}\text{Ne}$  atoms with a multichannel plate (MCP) detector. From these measurements (analogous to [19]) we can establish the ratio of the rate of ionizing inelastic collisions ( $\beta_{\text{ion}} \bar{n}$ ) to the total rate of inelastic collisions ( $\beta \bar{n}$ ):  $\beta_{\text{ion}}/\beta = 1.1(2)$ , where the uncertainty is dominated by the calibration uncertainty of the MCP detector. These measurements confirm, that the observed inelastic collisions are caused by Penning ionization to a very high degree ( $\geq 90\%$ ).

Our measurements prove the suppression of Penning ionization due to spin-polarization. Compared to  $\text{He}^*$  this suppression is much less pronounced. The observed values for  $\beta_{\text{unpol}}/\beta$  do not confirm that large suppression ratios are likely [12, 30]. We expect that refined calculations of the ionization rate with precise interaction potentials [27, 28] will reproduce the experimental results.

As a summary, Table I gives the collisional parameters for both neon isotopes as presented in this paper. With these measurements, a significant contribution towards the understanding of the collisional properties of spin-polarized metastable neon atoms is gained. These results will initiate further theoretical and experimental investigations, such as detailed calculations of the molecular potentials and their manipulation by external electromagnetic fields, e.g. to modify the rate of elastic or inelastic collisions. Concerning the quest for BEC, the determined ratio of elastic to inelastic collisions suggests  $^{22}\text{Ne}$  to be better suited for evaporative cooling than  $^{20}\text{Ne}$ . Accordingly, we have carried out first experiments of evaporative cooling of  $^{22}\text{Ne}$  and an increase in phase space density was already observed [18]. Whether a BEC

of  $^{22}\text{Ne}$  can be realized hereby, will be revealed by forthcoming evaporation experiments.

We thank A. Bunkowski and M. Johanning for valuable discussions and are grateful for financial support by the DFG (*Schwerpunktprogramm SPP 1116*) and the European Commission (*RTN Network Cold Quantum Gases*).

- 
- [1] M.J. Anderson et al., *Science* **269**, 198 (1995); K.B. Davis et al., *Phys. Rev. Lett.* **75**, 3969 (1995); C.C. Bradley et al., *Phys. Rev. Lett.* **78**, 985 (1997).
- [2] J.R. Anglin and W. Ketterle, *Nature* **416**, 211 (2002).
- [3] M. Greiner et al., *Nature* **426**, 537 (2003); S. Jochim et al., *Science* **302**, 2101 (2003); M.W. Zwierlein et al., *Phys. Rev. Lett.* **91**, 250401 (2003).
- [4] K. Burnett et al., *Nature* **416**, 225 (2002).
- [5] A. Robert et al., *Science* **292**, 461 (2001).
- [6] F. Pereira Dos Santos et al., *Phys. Rev. Lett.* **86**, 3459 (2001).
- [7] Y. Takasu et al., *Phys. Rev. Lett.* **91**, 040404 (2003).
- [8] P.O. Schmidt et al., *Phys. Rev. Lett.* **91**, 193201 (2003).
- [9] J. Werner et al., arXiv: cond-mat/0412409 (2004).
- [10] S. Seidelin et al., *Phys. Rev. Lett.* **93**, 090409 (2004).
- [11] J. Léonard et al., *Phys. Rev. Lett.* **91**, 073203 (2003).
- [12] M.R. Doery et al., *Phys. Rev. A* **58**, 3673 (1998).
- [13] V.P. Mogendorff et al., *Phys. Rev. A* **69**, 012706 (2004).
- [14] F.M. Penning, *Naturwissenschaften* **15**, 818 (1927).
- [15] C. Orzel et al., *Phys. Rev. A* **59**, 1926 (1999).
- [16] S.J.M. Kuppens et al., *Phys. Rev. A* **65**, 023410 (2002).
- [17] M. Zinner, Ph.D. thesis, Universität Hannover (2002).
- [18] P. Spoden, Ph.D. thesis, Universität Hannover (2004).
- [19] M. Zinner et al., *Phys. Rev. A* **67**, 010501 (2003).
- [20] P.O. Schmidt et al., *J. Opt. Soc. Am. B* **20**, 960 (2003).
- [21] C.R. Monroe et al., *Phys. Rev. Lett.* **70**, 414 (1993).
- [22] S.A. Hopkins et al., *Phys. Rev. A* **61**, 032707 (2000).
- [23] The full trapping potential of the magnetic trap beyond its harmonic approximation has to be used to determine  $\bar{n}$  accurately. In order to further study the influence of ergodic mixing, we conduct Monte Carlo simulations (similar to those of [31]) of the relaxation process in the full potential. As these simulations reproduce relaxation cross sections obtained from the theory of Kavoulakis et al. [24], ergodic mixing is irrelevant in our measurements.
- [24] G. Kavoulakis, C. Pethick, and H. Smith, *Phys. Rev. A* **61**, 053603 (2000).
- [25] Measurements were taken at magnetic offset fields of 5, 11, 15, and 25 G. We have no indication that the relaxation rate changes with the magnetic field in this range.
- [26] Intrinsic heating does not affect relaxation measurements since  $\dot{\sigma}_x/\sigma_x = \dot{\sigma}_r/\sigma_r$ , which leaves  $A$  unchanged.
- [27] S. Kotochigova, E. Tiesinga, and I. Tupitsyn, *Phys. Rev. A* **61**, 042712 (2000).
- [28] A. Derevianko and A. Dalgarno, *Phys. Rev. A* **62**, 062501 (2000).
- [29] J. Söding et al., *Phys. Rev. Lett.* **80**, 1869 (1998).
- [30] H.C.W. Beijerinck et al., *Phys. Rev. A* **61**, 023607 (2000).
- [31] H. Wu, E. Arimondo, and C.J. Foot, *Phys. Rev. A* **56**, 560 (1997).